Electrochemical performance and effect of moisture on Ba$_{0.5}$Sr$_{0.5}$Sc$_{0.175}$Nb$_{0.025}$Co$_{0.8}$O$_{3-\delta}$ oxide as a promising electrode for proton-conducting solid oxide fuel cells

Yidan Zhang[a, §], Ankang Zhu[a, §], Youmin Guo[a,*], Chunchang Wang[a], Meng Ni[b], Hao Yu[c], Chuanhui Zhang[d], Zongping Shao[e,f]

[a]School of Physics and Materials Science, Anhui University, No.111 Jiulong Road, Hefei, 230601 China

[b]Department of Building and Real Estate, The Hong Kong Polytechnic University, Hung Hom, Kowloon, Hong Kong, China

[c]College of Chemical and Environmental Engineering, Shandong University of Science and Technology, 266590, Qingdao, China

[d]Institute of Materials for Energy and Environment, School of Materials Science and Engineering, Qingdao University, Qingdao, 266071, PR China

[e]State Key Laboratory of Materials-Oriented Chemical Engineering, College of Chemistry and Chemical Engineering, Nanjing University of Technology, No.5 Xin Mofan Road, Nanjing, 210009, China

[f]Department of Chemical Engineering, Curtin University, Perth, Western Australia 6845, Australia

[§] These authors contributed equally to this work.

[*] Corresponding author: Y. Guo, Email: youminguo@ahu.edu.cn

Abstract

Proton conducting solid oxide fuel cells are solid state electrochemical devices for power generation at a conversion efficiency ($>$60%) higher than conventional thermal power plants ($\sim$40%). The cathode is the key component of proton conducting solid oxide fuel cells as it contributes to more than 50% of the total overpotential loss of an H$^+$-SOFC with thin film electrolyte. This work aims to develop high performance and durable cathode for proton conducting solid oxide fuel cells by doping Ba^{2+} into the Sr-site of the SrSc$_{0.175}$Nb$_{0.025}$Co$_{0.8}$O$_{3-\delta}$ perovskite oxide. The influence of moisture on the catalytic activity of Ba$_{0.5}$Sr$_{0.5}$Sc$_{0.175}$Nb$_{0.025}$Co$_{0.8}$O$_{3-\delta}$ cathode was investigated using electrochemical impedance spectroscopy of symmetric cell at 600 °C. The resistance in the low-frequency range was found to be the rate-limiting step of the oxygen

reduction reaction in the dry air, while the resistance in the medium-frequency range became the rate-limiting step in the moist air. With a $Ba_{0.5}Sr_{0.5}Sc_{0.175}Nb_{0.025}Co_{0.8}O_{3-\delta}$ cathode, a proton conducting single cell achieved good performance at a temperature of 700 °C with a power density of 633 mW cm^{-2}. However, the performance of single cell decreased with time, probably due to the agglomeration of cathode particles and the coverage of produced water on the active surface. To improve the durability of the proton conducting solid oxide fuel cell, it is critical to minimize the cathode particle agglomeration and remove the produced water effectively. The research results contribute to the development of high-performance fuel cell for efficient energy conversion.

Keywords Proton conducting solid oxide fuel cells; Co-doping; Cathode; Oxygen reduction reaction; Electrochemical impedance spectroscopy

1. Introduction

Because of the high efficiency, quiet operation, low emission and fuel flexibility, proton (H$^+$) conducting solid oxide fuel cells (H$^+$-SOFCs) are considered to be very promising power conversion devices[1, 2]. Compared to conventional SOFCs with an oxygen ion conduction (O^{2-}-SOFCs), H$^+$-SOFCs are more suitable for intermediate temperature (400-700 °C) operation due to their lower activation energy in this temperature range. In addition, the efficiency of H$^+$-SOFCs is potentially higher due to a higher fuel utilization since the fuel-diluting steam is produced in the cathode. Also, the danger of detrimental anode oxidation under high load condition can be avoided, indicating that H-SOFCs are beneficial to the more stable long-term operations. Furthermore, it has been successfully demonstrated that H-SOFCs have super anti-coking resistance in direct-hydrocarbon fuel operations [2]. However, the cell output cannot meet the requirements of industrial application due to the sluggish kinetic of the cathode of H$^+$-SOFCs. The cathode is the key to achieve high performance operation of H$^+$-SOFCs as more than 50% of the total overpotential loss comes from the cathode [3]. To develop high performance and durable cathode for H$^+$-SOFCs, it is of paramount importance to understand the key processes and rate-determining steps involved in the cathode operation. In general, there are three

main steps involved in the oxygen reduction reaction (ORR) occurring at the cathode of H^+-SOFCs [4, 5]: (1) charge transfer process alongside surface dissociative and diffusion of oxygen, (2) migration of proton from electrolyte to electrolyte-electrode-gas boundaries (TPBs) and (3) water generation and desorption at the cathode. The water formed on the cathode side may make the cathode reactions more complex and necessitate special requirements. So far, the exact influence of water formation at the electrode on the ORR activity of the cathode for H^+-SOFCs is still not clear[6, 7].

To date, materials used for the cathode of H^+-SOFCs could be classified into four types according to their conducting species: pure electronic (e^-) conductors (PECs), mixed oxygen ionic and electronic (O^{2-}/e^-) conductors (MIECs), mixed protonic and electronic (H^+/e^-) conductors (MPECs) and triple conducting ($O^{2-}/e^-/H^+$) oxides (TCOs) [5, 8]. When PECs are used as cathodes, such as Pt, electroactive oxygen is diffused along the Pt surface to TPBs, and hence, the dissociated oxygen ions react with H^+ to produce water, resulting in the reaction areas being limited to TPBs and thus a low active site density[9]. When MIECs are applied as cathodes, the introduced O^{2-} expands the transfer paths of electroactive oxygen to TPBs[10, 11]. When MPECs are used as cathodes, the TPBs for water evolution reactions are extended to the entire interface of gas/electrode and favor the cathode reaction[12, 13]. However, the concentration of transition metals in MPEC oxides is quite limited, which results in poor electrocatalytic activity to ORR and lower performances than PEC and MIEC materials[8, 12]. To further increase the number of electrochemically active sites, cathodes with TCOs are developed [14]. By applying TCOs as the cathode, the TPBs of electrode are expanded to the electrode bulk, significantly promoting the transfer and reaction of protons with oxygen species[15, 16]. However, the electrode materials with TCOs reported for H^+-SOFCs are very limited. Although composite oxides with TCOs can be obtained by mixing a MIEC cathode with a proton-conducting electrolyte, a phase reaction of MIEC oxide with proton-conducting electrolyte may occur, producing undesired phases[17-19]. Therefore, developing a strategy to improve the cathode process for ORR is still critical for improving the performance of H^+-SOFCs.

Recently, we have demonstrated that the electrode reaction of the $SrSc_{0.175}Nb_{0.025}Co_{0.8}O_{3-\delta}$ (SSNC) MIEC oxide on H^{+}-SOFCs can be improved by introducing H_2O into the air atmosphere[20]. The polarization resistance (R_p) and ohmic resistance (R_o) were simultaneously reduced when water was introduced into the cathode side. This phenomenon could be caused by the *in situ* generation of proton in the SSNC cathode. However, an interfacial reaction between SSNC and Zirconium and Yttrium co-doped $BaCeO_3$ electrolyte was also detected[20]. As reported in the literature, partial replacement of Sr^{2+} with Ba^{2+} in the A-site of perovskite can improve its phase stability [21]. In addition, this substitution also improves electronic and oxygen ionic conductivity of perovskite, which has a significant influence on the catalytic activity of the cathode[22]. Thus, doping Ba into the Sr-site of SSNC could potentially improve the activity and stability of SSNC cathode for H^{+}-SOFCs. However, the current literature is lacking relevant study and it is unknown how the doping of Ba can influence the performance of the SSNC cathode. In this work, new H^{+}-SOFC cathode material was synthesized and investigated systematically by doping Ba^{2+} into the Sr-site of SSNC to form $Ba_{0.5}Sr_{0.5}Sc_{0.175}Nb_{0.025}Co_{0.8}O_{3-\delta}$ (BSSNC). The phase structure, chemical compatibility, electrical conductivity and electrocatalytic activity of BSSNC materials were measured. This study also optimized the H^{+}-SOFCs performance and stability by explaining the effect of moisture on the BSSNC cathode. The research results are critical for developing high performance and durable H^{+}-SOFC cathode for sustainable and efficient energy conversion.

2. Material and methods

$Ba_{0.5}Sr_{0.5}Sc_{0.175}Nb_{0.025}Co_{0.8}O_{3-\delta}$ (BSSNC) powders were prepared using a sol-gel route. For synthesis of BSSNC oxide, high-purity agents of Barium nitrate, Strontium nitrate, Scandium nitrate from Sinopharm Chemical Regent, were mixed with Niobium oxalate hydrate and Cobalt nitrate hexahydrate from Aladdin Regents in water according to the stoichiometric ratio. Then EDTA and citric acid were mixed in deionized water at room temperature, and ammonia was added to the mixture of EDTA and CA to neutralize the solution. The solution of EDTA and CA was dropped to metal ions solution with stirring to form an aqueous solution with a pH of ~8[20].

The solution was evaporated and transparent gel was got, and then pre-fired to obtain ash at 260 °C [23]. The as-prepared ash was calcined in air to obtain BSSNC oxide. The synthesis of $BaZr_{0.1}Ce_{0.7}Y_{0.2}O_{3-\delta}$ (BZCY) was similar to those described previously[24]. The sintering temperature were set as 1000 °C. The chemical compatibility of BSSNC with BZCY was investigated by mixing samples and sintering at various temperatures. Phase structure of the synthesized BSSNC, BZCY and BSSNC-BZCY composites after treatment under different conditions were characterized using X-ray diffraction (XRD, Smartlab). Their phases structures were also determined via Fourier transform-infrared spectroscopy (FTIR, VERTEX80). The electrical conductivity of dense BSSNC bar was measured at 300-800 °C and different air conditions as reported in our recent work[20]. Temperature-programmed desorption of oxygen (O_2-TPD) measurements of BSSNC and SSNC powder were performed on an automated chemisorption analyzer. The oxygen desorption was done in a quartz reactor. Before the O_2-TPD run, powders were pretreated in synthetic air at 850 °C for 2 h. During the desorption process, the sample was heated up to 950 °C at 10 °C min^{-1}. Meanwhile, He gas with a flow rate of 25 mL min^{-1} was flowed into the reactor. The desorbed oxygen signal was simultaneously recorded using Thermal Conductor Detector (TCD). Electrochemical performance of BSSNC was studied by preparing BSSNC/BZCY/BSSNC symmetrical cells and NiO+BZCY/BZCY/BSSNC single cells as reported in our recent work[20]. A scanning electron microscope was applied to analyze the microstructure of the cathode/electrolyte interface.

3. Results and discussion

Fig. 1a presents the XRD pattern of synthesized BSSNC. The BSSNC powder exhibits diffraction peaks corresponding to cubic structure. The calculated lattice constant for BSSNC was 4.016 Å, which was higher than that of SSNC (3.908 Å). The lattice constant was increased after doping of Ba^{2+} into the A-site of the SSNC structure, because the ionic radius of 12-corrdinated Ba^{2+} is larger than that of 12-cordinated Sr^{2+}. The result suggested that Sr^{2+} in SSNC was successfully

substituted by Ba^{2+} with the formation of a pure BSSNC structure by the sol-gel process.
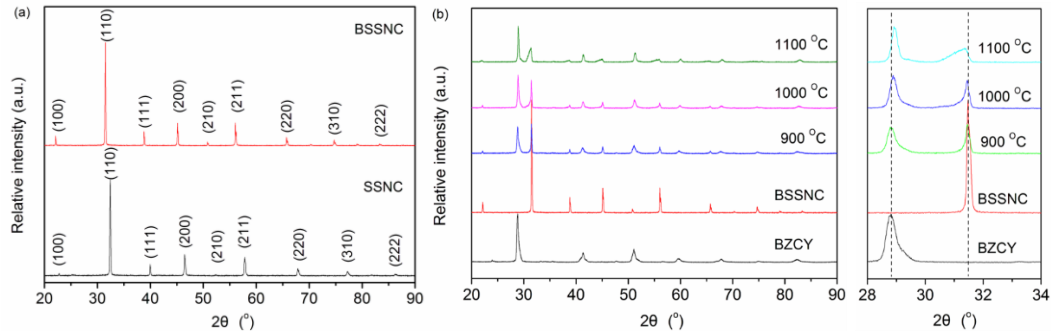

Fig. 1. (a) XRD patterns of synthesized BSSNC oxide after sintering; (b) XRD patterns of the BSSNC-BZCY mixture fired at 900, 1000 and 1100 °C.

Fig. 1b shows the XRD patterns of BSSNC-BZCY mixtures (1:1) after firing at 900, 1000 or 1100 °C for 5 h. The mixture was well indexed according to the major diffraction peaks of BSSNC and BZCY after firing at 900 °C. There was no discernible shift in either the BSSNC or BZCY peaks. However, the sharp peaks of both BSSNC and BZCY shifted slightly at 1000 °C, and this shift intensified when the reaction temperature was further increased to 1100 °C. This phenomenon was likely attributable to the cation exchange between BSSNC and BZCY, similar to the phenomenon observed in the SSNC-BZCY mixture[20]. During the firing process at high temperature, Ba^{2+} in BZCY diffused into the A-site of BSSNC, resulting in the lattice expansion of the BSSNC phase and lattice shrinkage of the BZCY phase. However, unlike that in the SSNC-BZCY mixture, this cation exchange in the BSSNC-BZCY mixture occurred only slightly after firing at the same temperature of 1000 °C[20]. This result confirmed that the chemical compatibility of BSSNC to BZCY electrolyte was improved by replacing Sr^{2+} with Ba^{2+}, which was consistent with the reported literature[21]. A high temperature is generally required to ensure sufficient contact between the BZCY electrolyte and BSSNC cathode. Therefore, the sprayed BSSNC cathode layer was fired at 1000 °C in this study to ensure good contact and avoid cation exchange.
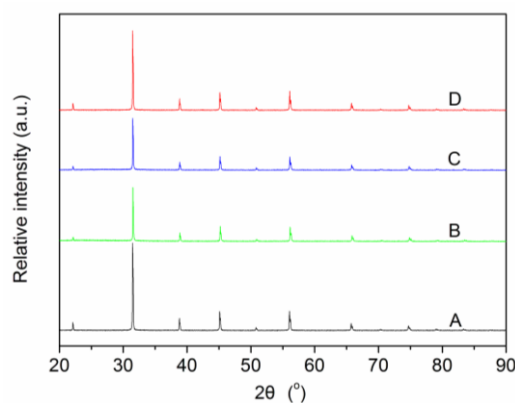
Fig. 2. XRD patterns of fresh BSSNC powder (A) and BSSNC powder treated in dry O_2 (B), 10% H_2O-O_2 (C) and 10% H_2O-air atmospheres (D) at 700 °C for 10 h.
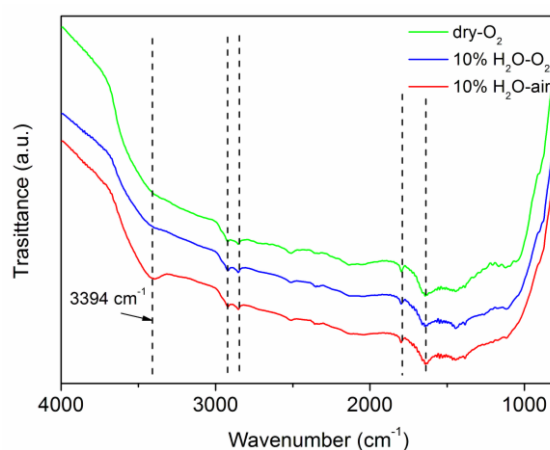

Fig. 3. Infrared (IR) spectra of BSSNC powder samples treated in different atmospheres.

To further evaluate the chemical activity of BSSNC in a moist air, BSSNC powders were exposed to a moist air containing 10% H_2O at 700 °C for 10 h. According to our previous work, strontium carbonate/strontium hydroxide was formed in SSNC when SSNC powder was exposed to air[20]. To eliminate the influence of CO_2 gas, BSSNC powder samples were also exposed to both a 10% H_2O-O_2 atmosphere and a dry O_2 at a temperature of 700 °C. All diffraction peaks of the treated BSSNC powder samples were well matched to those of fresh BSSNC phases, and no other phases appeared (**Fig. 2**). This result suggests that the BSSNC is more stable than SSNC in moist environments at a high temperature. The above conclusion was also proven by FT-IR data. **Fig. 3** shows the IR spectra of the BSSNC powder samples after treatment in dry O_2, 10% H_2O-O_2 and 10% H_2O-air at 700 °C for 10 h. Unlike the spectrum reported for SSNC, the IR spectra of the BSSNC

7

samples after treatment in different atmospheres exhibited no obvious adsorption band corresponding to CO_3^{2-}. The adsorption band at 3944 cm^{-1} was observed in the BSSNC sample after the exposure in the H_2O-containing atmosphere, and this band can be indexed to the OH$^-$ stretch, in agreement with the result reported for SSNC[20]. These findings demonstrated that the chemical stability of BSSNC was also improved after the partial replacement of Sr^{2+} by Ba^{2+}. The operational stability of BSSNC when used as the cathode of a single cell is discussed in further detail below.
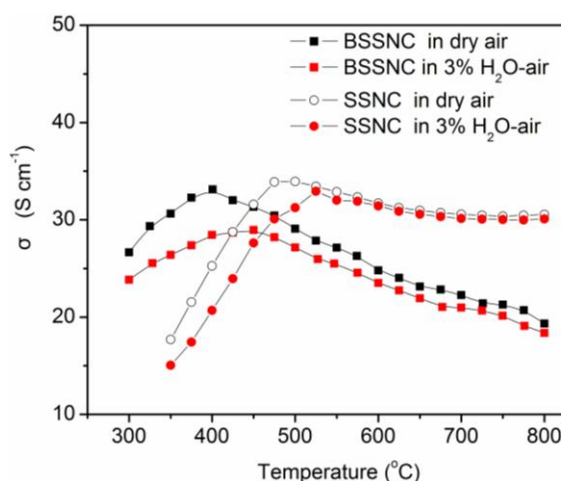

Fig. 4. Total electrical conductivities of BSSNC oxide under air with different water partial pressures.

Fig. 4 presents the total electrical conductivity of the BSSNC perovskite increased with increasing temperature below 400 °C and then presented a downward trend with a further increase in temperature above 400 °C in dry air. A recent study reported that $S_{1-x}SNC$ showed semiconducting behavior below ~475 °C and metallic behavior above ~475 °C[25]. BSSNC had a very similar maximum value of electrical conductivity as that of SSNC (~34 S cm^{-1} under dry air); however, BSSNC showed a lower conductivity than SSNC under the corresponding conditions above the transition temperature [20]. This decrease in the electrical conductivity of BSSNC can be ascribed to more favorable electrical compensation by creating oxygen vacancies[21]. Meanwhile, the electrical conductivity of BSSNC may be decreased as a result of the overlapping degree between B-O-B bonds. The BSSNC oxide has larger B-O distance than that of SSNC, which causes more difficult electron hopping. In addition, the transition temperature was reduced by the introduction of Ba^{2+} into the

A-site of SSNC. This reduction in transition temperature (Ts) may be a sign of the high kinetics of surface-exchange and oxygen bulk diffusion at lower temperatures. However, smaller values of the total electrical conductivities of BSSNC were obtained after introducing 3% H_2O into the air atmosphere, and the maximum value was 28 S cm^{-1} at 450 °C. We also have to note that the introduction of proton conductivity can lead to a decrease in electronic conductivity. For perovskite oxides, the electronic conductivity is generally considered to be overwhelming compared to its ionic conductivity. Thus, it is difficult to monitor the effect of H_2O partial pressure on the total conductivity as the ion conduction contributes insignificantly to the total conductivity.
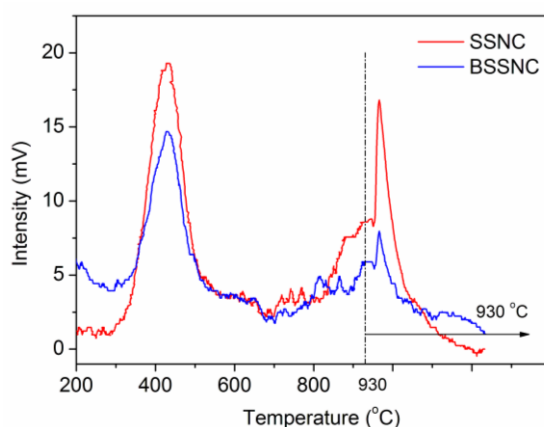

Fig. 5. O_2-TPD profiles of synthesized SSNC and BSSNC.

Oxygen desorption experiment was performed to study the influence of Ba^{2+} doping on the nature of the oxygen species and their mobility. **Fig. 5** shows the oxygen desorption profiles of BSSNC and SSNC. There are two desorption peaks in the intermediate temperature range (300-700 °C, peak I) and high temperature range (>800 °C, peak II). Both peaks could contribute to the desorption of lattice oxygen. The desorption peak I is attributed to the reduction Co^{4+} →Co^{3+} in the oxide lattice, whereas the peak II corresponding to the further reduction Co^{3+} →Co^{2+}[26]. The area of peak corresponds to the concentration of various metal cations in the oxides. Thus, the amounts of desorbed oxygen were calculated by quantitative integration method. BSSNC exhibited weaker intensity (0.15 mmol g^{-1} of peak I and 0.11 mmol g^{-1} of peak II) than that of the SSNC sample (0.24 mmol g^{-1} in Region I and 0.20 mmol g^{-1} in Region II). This result demonstrated that Ba^{2+} doping caused

9

changes in the structure of the oxygen species, which could lead to different ORRs when BSSNC was applied as the cathode of H^+-SOFC. The following work will focus on the electrochemical performance of BSSNC electrode.

Fig. 6a presents the electrochemical resistances of the BSSNC/BZCY/BSSNC cells in dry- and 3% H_2O-air. High ohmic resistance (R_o) was observed in our study due to the thick BZCY electrolyte film (0.48 mm in thickness). With adding moisture water to the dry air, both R_o and polarization resistance (R_p) decreased. For instance, the R_o value decreased from 4.26 to 3.47 Ω cm^{-2}, while the R_p decreased from 1.46 to 0.66 Ω cm^{-2} in 3% H_2O-air at 600 °C. These observed decrease in R_o may be ascribed to the promoted proton transfer between BZCY electrolyte and BSSNC electrode, which was activated by adsorbed water molecule on the surface of BZCY electrolyte[20, 27]. In addition, the water intake on the BSSNC cathode was involved in the oxygen reduction reaction and facilitated its reaction, resulting in the decrease of R_p[20, 27]. The influence of moisture on the electrochemical performance of BSSNC electrode was further investigated by comparing the impedance spectra in a symmetric cell configuration under various moisture conditions. As shown in **Fig. 6b**, a continuous decrease in R_o from 3.47 to 3.19 Ω cm^{-2} was observed with increasing the moisture content from 3% to 20%. In contrast, R_p decreased first to approximately 0.58 Ω cm^{-2} in 5% H_2O-air and then increased back to 0.66 Ω cm^{-2} in 20% H_2O-air. This decrease in R_o and R_p in moist air may be attributed to the enhanced H^+ conduction in the BZCY and BSSNC oxides[20]. However, in moist air with a high H_2O partial pressure (for example 20%), excess water may cover the surface of the BSSNC particles, resulting in the reduction in active sites for oxygen molecules adsorption/dissociation and thereby leading to a high R_p[28].
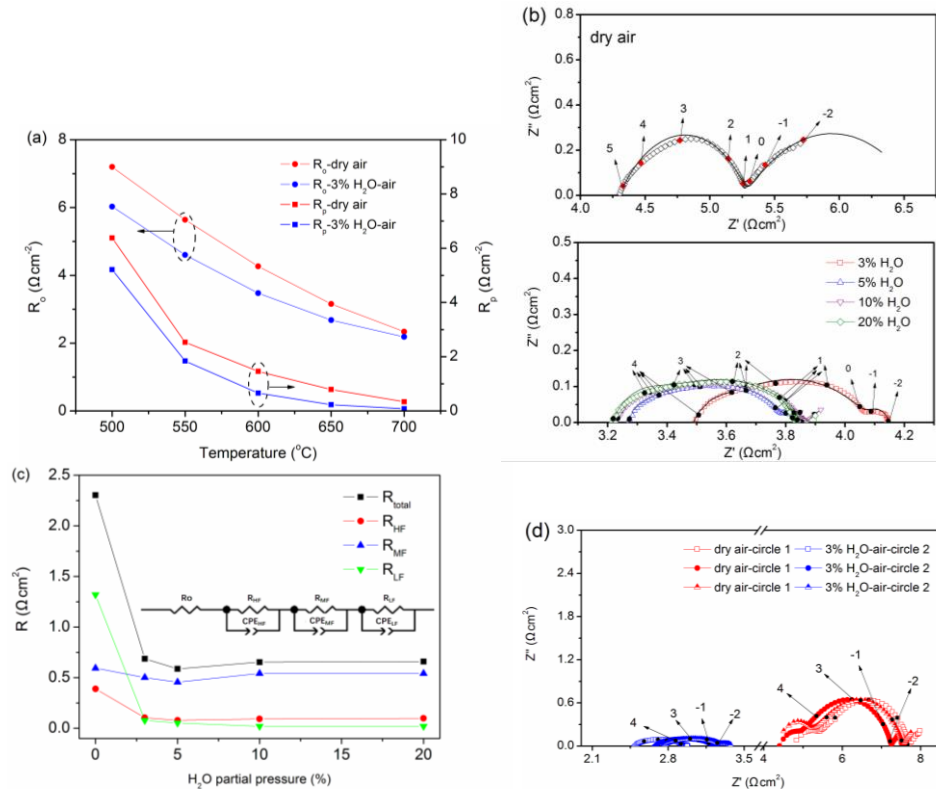
Fig. 6. (a) The ohmic resistance (Ro) and polarization resistance (Rp) of the BSSNC/BZCY/BSSNC cells in dry air and 3% H_2O-air; (b) Electrochemical impedance spectra of the symmetrical cells in various H_2O partial pressures at 600 °C. The open scatters present the experimental data and the solid lines are the fitted curves. (c) The fitting values of the electrochemical impedance spectra at 600 °C; and (d) Impedance spectra of BSSNC/BZCY/BSSNC symmetrical cells recorded in dry air and 3% H_2O-air with loop.

We further to identify the rate-limiting step in the electrochemical reactions of BSSNC cathode by resolving the EIS spectra with the inserted equivalent circuit. The high-frequency (HF, $\sim10^6$ to $\sim10^4$ Hz) range is ascribed to the charge transfer processes and includes ion- and electron-transfer through the interfaces of electrode/electrolyte and the current collector/electrode. The middle-frequency (MF, $\sim10^4$ to $\sim10^0$ Hz) range corresponds to molecular dissociation of adsorbed O_2 (O_2 (ads)). The low-frequency (LF, $\sim10^0$ to $\sim10^{-2}$ Hz) range is related to the diffusion processes[5, 8, 14, 28]. As shown in **Fig. 6c**, in dry air, the R_{LF} accounted for the largest proportion, suggesting that the diffusion process was the rate-limiting step. In moist air, all the resistances decreased, especially the R_{LF}, and the R_{MF} became the main resistance component. As pointed out by R. Peng et al., the change in R_{LF} is

11

considerably related to the microstructure, the components, the conducting species as well as conductivities of the cathode materials. In this study, the obvious decrease in R_{LF} can be ascribed to water insertion, justifying that the ORR was enhanced by water intake capability of the BSSNC cathode[28]. Another possible reason for the reduction in R_{LF} is the lower oxygen content resulting from the increase in moisture. The decrease in R_{MF} illustrated the faster kinetics of the molecular dissociation of adsorbed O_2 when moisture was introduced. However, both R_{HF} and R_{MF} tended to increase when over 5% moisture was introduced. This may be attributable to the excess water on the catalyst surface, which affects the H_2O desorption and charge transfer processes. As a result, it can be reasonably postulated that the oxygen molecule dissociation from the BSSNC is the rate-limiting step of the electrode reaction in moist air. In addition, BSSNC is characterized by MIEC behavior, and excess water is mainly generated in the internal area between electrolyte and electrode interface, which could block the ion- and electron-transfer processes. **Fig. 6d** gives impedance spectra of BSSNC/BZCY/BSSNC cells tested in dry air and 3% H_2O-air with loop. Obviously, the R_o and R_p ultimately reached a relatively stable state in the wet and dry cycle tests. This further confirmed that the presence of water in air played a key role in the oxygen reduction processes of BSSNC cathode. The water uptake may introduce proton conduction in the bulk of BSSNC cathode, changing the rate-limiting step and subsequently facilitating the electrode kinetics.
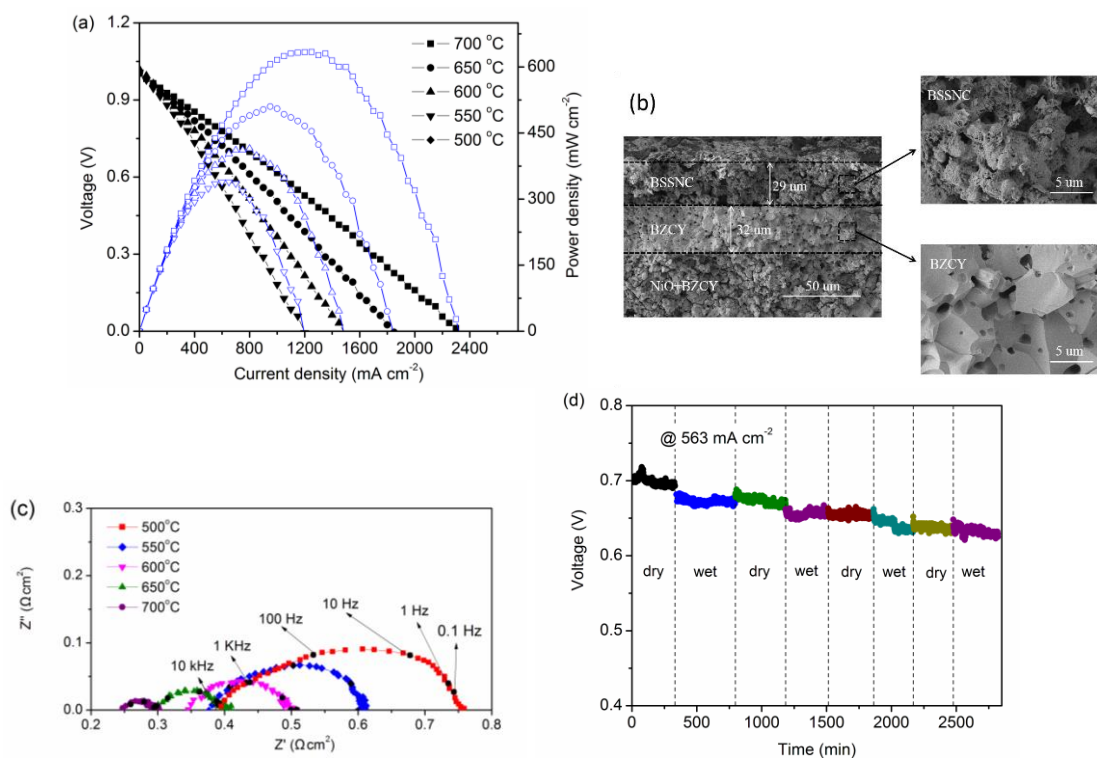
Fig. 7. (a) Cell performance of a single fuel cell with a BSSNC cathode sintered at 1000 °C; (b) Morphology of the cell after the I-V polarization tests; (c) EIS of the single fuel cell under open circuit voltage; (d) Cyclic stability test of the fuel cells at I=563 mA cm^{-2} at 700 °C.

To evaluate the fuel cell performance under real fuel cell operating condition, single cells with a BSSNC cathode were fabricated. As shown in **Fig. 7a**, the cell showed a good performance at 700 °C with a peak power density of 633 mW cm^{-2} when it was operated on H_2 in the NiO+BZCY anode and synthetic air (80 mL min^{-1} under standard atmospheric pressure) containing 3% H_2O in the BSSNC cathode. As shown in **Fig. 7b**, the BZCY electrolyte film was 32 μm, and the BSSNC layer was 29 μm. The cell has an ideal thickness of BSSNC electrode layer, which may ensure good fuel cell performance[29]. **Fig. 7c** presents the corresponding EIS of the single cells under OCV. The R$_o$ of 0.34 Ω cm^{-2} and the R$_p$ of 0.17 Ω cm^{-2} were observed at 600 °C. The result further confirmed that the BSSNC oxide can be used as a cathode for H$^+$-SOFC applications. **Fig. 7d** shows the cyclic stability test for the symmetrical cells in dry air and 3% H_2O-air operating with I= 563 mA cm^{-2}. It is clearly observed that the voltage decreased over time regardless of what atmosphere was applied on the cathode side. The most likely reason for the performance degradation is the agglomeration and/or coarsening of electrocatalysts in the cathode. A more detailed

analysis of the curves revealed that the voltage decreased faster in the moist air than in the dry air. The possible reason for this phenomenon was that a large amount of water was produced on the cathode side when the cell was operated under a high current density. This produced water could cover the cathode reaction sites, resulting in the degradation of fuel cell performance. The results indicated that the agglomeration of the cathode, concurrent with the reduced cathode reaction surface covered by produced water, contributes to the degradation of fuel cell performance. Further analysis is needed to determine the microstructure of the cathode at which the water produced and the effect of microstructure, if any, on the overall performance of the cathode. The operation stability of the fuel cell can be improved for real application by optimizing the operation condition and decorating the microstructure of cathode.

4. Conclusions

The compatibility and stability were successfully promoted via doping Ba^{2+} into the Sr-site of the $SrSc_{0.175}Nb_{0.025}Co_{0.8}O_{3-\delta}$ perovskite with the synthesis of $Ba_{0.5}Sr_{0.5}Sc_{0.175}Nb_{0.025}Co_{0.8}O_{3-\delta}$. The BSSNC material was also stable under moist air with high water partial pressure. For a symmetrical cell with $Ba_{0.5}Sr_{0.5}Sc_{0.175}Nb_{0.025}Co_{0.8}O_{3-\delta}$ electrodes, the ohmic and polarization resistances decreased simultaneously when an appropriate amount of moisture was introduced. This result coincided well with the typical hydration behavior of the $BaZr_{0.1}Ce_{0.7}Y_{0.2}O_{3-\delta}$ electrolyte and the increased proton conduction in the $BaZr_{0.1}Ce_{0.7}Y_{0.2}O_{3-\delta}$ electrolyte and $Ba_{0.5}Sr_{0.5}Sc_{0.175}Nb_{0.025}Co_{0.8}O_{3-\delta}$ electrodes. However, excess water could suppress the adsorption/dissociation of oxygen molecules, leading to high polarization resistance. Further investigation illustrated that the rate-limiting step of oxygen reduction reaction at $Ba_{0.5}Sr_{0.5}Sc_{0.175}Nb_{0.025}Co_{0.8}O_{3-\delta}$ cathode on $BaZr_{0.1}Ce_{0.7}Y_{0.2}O_{3-\delta}$ electrolyte was changed from oxygen diffusion processes in dry air to oxygen molecule dissociation in moist air. A maximum power density generated with $Ba_{0.5}Sr_{0.5}Sc_{0.175}Nb_{0.025}Co_{0.8}O_{3-\delta}$ cathode was 633 mW cm^{-2} at 700 °C. However, the

cell performance degraded over time during the cycling stability test in the dry air and moist air atmospheres. This work demonstrated that the role of water in the cathode materials must be considered, when designing and developing alternative cathodes for proton conducting solid oxide fuel cells.

Acknowledgments

References

[1] L. Bi, E. Fabbri, E. Traversa, Solid oxide fuel cells with proton-conducting $La_{0.99}Ca_{0.01}NbO_4$ electrolyte, Electrochim Acta, 260 (2018) 748-754.
[2] H. Xu, B. Chen, P. Tan, W. Cai, W. He, D. Farrusseng, et al, Modeling of all porous solid oxide fuel cells, Appl Energ, 219 (2018) 105-113.
[3] L. Lei, J.M. Keels, Z. Tao, J. Zhang, F. Chen, Thermodynamic and experimental assessment of proton conducting solid oxide fuel cells with internal methane steam reforming, Appl Energ, 224 (2018) 280-288.
[4] F. He, T. Wu, R. Peng, C. Xia, Cathode reaction models and performance analysis of $Sm_{0.5}Sr_{0.5}CoO_{3-\delta}$-$BaCe_{0.8}Sm_{0.2}O_{3-\delta}$ composite cathode for solid oxide fuel cells with proton conducting electrolyte, J Power Sources, 194 (2009) 263-268.
[5] R. Peng, T. Wu, W. Liu, X. Liu, G. Meng, Cathode processes and materials for solid oxide fuel cells with proton conductors as electrolytes, J Mater Chem, 20 (2010) 6218-6225.
[6] A. Grimaud, J.M. Bassat, F. Mauvy, M. Pollet, A. Wattiaux, M. Marrony, J.-C. Grenier, Oxygen reduction reaction of $PrBaCo_{2-x}Fe_xO_{5+\delta}$ compounds as H^+-SOFC cathodes: correlation with physical properties, J Mater Chem A, 2 (2014) 3594.
[7] W. Wang, D. Medvedev, Z. Shao, Gas humidification impact on the properties and performance of perovskite-Type functional materials in proton-conducting solid oxide cells, Adv Funct Mater, 28 (2018) 1802592.
[8] Y. Lin, R. Ran, C. Zhang, R. Cai, Z. Shao, Performance of $PrBaCo_2O_{5+\delta}$ as a proton-conducting solid-oxide fuel cell cathode, J Phys Chem A, 114 (2010) 3764-3772.

[9] H. Uchida, S. Tanaka, H. Iwahara, Polarization at Pt electrodes of a fuel cell with a high temperature-type proton conductive solid electrolyte, J Appl Electrochem, 15 (1985) 93-97.

[10] K. Zhang, L. Ge, R. Ran, Z. Shao, S. Liu, Synthesis, characterization and evaluation of cation-ordered $LnBaCo_2O_{5+\delta}$ as materials of oxygen permeation membranes and cathodes of SOFCs, Acta Mater, 56 (2008) 4876-4889.

[11] N. Ortiz-Vitoriano, C. Bernuy-López, I. Ruiz de Larramendi, R. Knibbe, K. Thydén, A. Hauch, P. Holtappels, T. Rojo, Optimizing solid oxide fuel cell cathode processing route for intermediate temperature operation, Appl Energ, 104 (2013) 984-991.

[12] Z. Tao, L. Bi, L. Yan, W. Sun, Z. Zhu, R. Peng, W. Liu, A novel single phase cathode material for a proton-conducting SOFC, Electrochem Commun, 11 (2009) 688-690.

[13] Z. Hui, P. Michele, Preparation, chemical stability, and electrical properties of $Ba(Ce_{1-x}Bi_x)O_3$ (x = 0.0-0.5), J Mater Chem, 12 (2002) 3787-3791.

[14] L. Fan, P.C. Su, Layer-structured $LiNi_{0.8}Co_{0.2}O_2$: A new triple ($H^+/O^{2-}/e^-$) conducting cathode for low temperature proton conducting solid oxide fuel cells, J Power Sources, 306 (2016) 369-377.

[15] J. Kim, S. Sengodan, G. Kwon, D. Ding, J. Shin, M. Liu, G. Kim, Triple-conducting layered perovskites as cathode materials for proton-conducting solid oxide fuel cells, ChemSusChem, 7 (2014) 2811-2815.

[16] D. Chen, Q. Zhang, L. Lu, V. Periasamy, M.O. Tade, Z. Shao, Multi scale and physics models for intermediate and low temperatures H^+-solid oxide fuel cells with $H^+/e^-/O^{2-}$ mixed conducting properties: Part A, generalized percolation theory for LSCF-SDC-BZCY 3-component cathodes, J Power Sources, 303 (2016) 305-316.

[17] E. Fabbri, A. D'Epifanio, E. Di Bartolomeo, S. Licoccia, E. Traversa, Tailoring the chemical stability of $Ba(Ce_{0.8-x}Zr_x)Y_{0.2}O_{3-\delta}$ protonic conductors for Intermediate Temperature Solid Oxide Fuel Cells (IT-SOFCs), Solid State Ionics, 179 (2008) 558-564.

[18] E. Fabbri, S. Licoccia, E. Traversa, E.D. Wachsman, Composite cathodes for proton conducting electrolytes, Fuel Cells, 9 (2009) 128-138.

[19] L. Yang, Z. Liu, S. Wang, Y. Choi, C. Zuo, M. Liu, A mixed proton, oxygen ion, and electron conducting cathode for SOFCs based on oxide proton conductors, J Power Sources, 195 (2010) 471-474.

[20] A. Zhu, G. Zhang, T. Wan, T. Shi, H. Wang, M. Wu, C. Wang, S. Huang, Y. Guo, H. Yu, Z. Shao, Evaluation of $SrSc_{0.175}Nb_{0.025}Co_{0.8}O_{3-\delta}$ perovskite as a cathode for proton-conducting solid oxide fuel cells: The possibility of in situ creating protonic conductivity and electrochemical performance, Electrochim Acta, 259 (2018) 559-565.

[21] P. Zeng, Z. Chen, W. Zhou, H. Gu, Z. Shao, S. Liu, Re-evaluation of $Ba_{0.5}Sr_{0.5}Co_{0.8}Fe_{0.2}O_{3-\delta}$ perovskite as oxygen semi-permeable membrane, J Membrane Sci, 291 (2007) 148-156.

[22] M. Søgaard, P. Vang Hendriksen, M. Mogensen, Oxygen nonstoichiometry and transport properties of strontium substituted lanthanum ferrite, J Solid State Chem, 180 (2007) 1489-1503.

[23] Y. Guo, H. Shi, R. Ran, Z. Shao, Performance of $SrSc_{0.2}Co_{0.8}O_{3-\delta}+Sm_{0.5}Sr_{0.5}CoO_{3-\delta}$ mixed-conducting composite electrodes for oxygen reduction at intermediate temperatures, Int J Hydrogen Energ, 34 (2009) 9496-9504.

[24] T. Wan, A. Zhu, Y. Guo, C. Wang, S. Huang, H. Chen, G. Yang, W. Wang, Z. Shao, Co-generation of electricity and syngas on proton-conducting solid oxide fuel cell with a perovskite layer as a precursor of a highly efficient reforming catalyst, J Power Sources, 348 (2017) 9-15.

[25] G. Chen, J. Sunarso, Y. Wang, C. Ge, J. Yang, F. Liang, Evaluation of A-site deficient $Sr_{1-x}Sc_{0.175}Nb_{0.025}Co_{0.8}O_{3-\delta}$ (x=0, 0.02, 0.05 and 0.1) perovskite cathodes for intermediate-temperature solid oxide fuel cells, Ceram Int, 42 (2016) 12894-12900.

[26] Y. Guo, D. Chen, H. Shi, R. Ran, Z. Shao, Effect of Sm^{3+} content on the properties and electrochemical performance of $Sm_xSr_{1-x}CoO_{3-\delta}$ ($0.2 \leq x \leq 0.8$) as an oxygen reduction electrodes on doped ceria electrolytes, Electrochim Acta, 56 (2011) 2870-2876.

[27] A. Grimaud, F. Mauvy, J.M. Bassat, S. Fourcade, L. Rocheron, M. Marrony, J.C. Grenier, Hydration Properties and Rate Determining Steps of the Oxygen Reduction Reaction of Perovskite-Related Oxides as H^+-SOFC Cathodes, J Electrochem Soc, 159 (2012) B683-B694.

[28] S. Sun, Z. Cheng, Effects of H_2O and CO_2 on electrochemical behaviors of BSCF cathode for proton conducting IT-SOFC, J Electrochem Soc, 164 (2017) F81-F88.

[29] Y. Guo, Y. Liu, R. Cai, D. Chen, R. Ran, Z. Shao, Electrochemical contribution of silver current collector to oxygen reduction reaction over $Ba_{0.5}Sr_{0.5}Co_{0.8}Fe_{0.2}O_{3-\delta}$ electrode on oxygen-ionic conducting electrolyte, Int J Hydrogen Energ, 37 (2012) 14492-14500.